*Aust. J. Phys.*, 1996, **49**, 39–49

# On the Lifetimes of Antisteady States*

*Debra J. Searles and Denis J. Evans*

Research School of Chemistry, Australian National University,
Canberra, ACT 0200, Australia.

*Abstract*

The influence of Lyapunov instability on the lifetimes of antisteady states is investigated using nonequilibrium molecular dynamics simulations. It is found that the lifetime is inversely proportional to the smallest Lyapunov exponent of the steady state system and proportional to the logarithm of the trajectory error per timestep.

## 1. Introduction

If one applies a dissipative force to a thermostatted $N$-particle system one can often generate a nonequilibrium steady state. An example might be low Reynolds number shear flow between thermostatted walls. In the nonequilibrium molecular dynamics SLLOD algorithm which employs Lees–Edwards periodic boundary conditions and a reversible deterministic thermostat, one calculates the material properties of shearing systems in a homogeneous fashion (Evans and Morriss 1990). The shearing motion is induced by the shearing periodic boundary conditions rather than by moving walls. The viscous heat is removed by employing a homogeneous thermostat derived from Gauss' Principle of Least Constraint rather than by conduction to the thermostatted walls.

In the linear regime close to equilibrium it has been proved (Evans and Morriss 1990) that the properties of the simulated system are identical to those of a corresponding real fluid flowing between moving thermostatted walls. In the absence of the thermostat it has been proved that the adiabatic SLLOD equations of motion give an exact description of adiabatic shear flow even far from equilibrium (Evans and Morriss 1990).

Like real experimental systems thermostatted SLLOD dynamics is time reversible. Thus one can then apply a time reversal mapping, $M^{\mathrm{T}}$, to the phase $\boldsymbol{\Gamma} = (x_1, y_1, z_1, x_2 \dots\ p_{xN}, p_{yN}, p_{zN})$ and shear rate $\gamma$ of the system, $M^{\mathrm{T}}[\boldsymbol{\Gamma}, \gamma] = [(x_1, y_1, z_1, x_2 \dots\ -p_{xN}, -p_{yN}, -p_{zN}), -\gamma]$, and the system will retrace its path. Such a process becomes very interesting if it is applied to phases which are typical of nonequilibrium steady states. In nonequilibrium steady

* Refereed paper based on a contribution to the fourth Gordon Godfrey Workshop on Atomic and Electron Fluids, held at the University of New South Wales, Sydney, in September 1994.

0004-9506/96/010039$05.00

states one invariably finds that the thermostat removes heat generated irreversibly by the dissipative field. This is of course consistent with the Second Law of Thermodynamics.

However, if one applies a time reversal mapping to a typical steady state phase, then from the properties of the mapping and the reversibility of the equations of motion we know that the system must retrace its path. If the initial path was, as we have assumed, entropy producing, then the retraced path must be entropy absorbing. We call such a trajectory an antisteady state trajectory. In the antisteady state the thermostat supplies heat which is converted into work in defiance of the Second Law.

In practice one cannot integrate the equations of motion of any system exactly. Computer simulations always have finite accuracy and experiments can never be completely isolated from uncontrolled external perturbations. So what one observes in practice is that after the application of the time reversal mapping an antisteady state is only followed for a finite time. Eventually the perturbation errors grow and the antisteady state decays into a positive entropy producing steady state, satisfying the Second Law.

In this paper we characterise the lifetime of antisteady states and the dependence of this lifetime on trajectory error and trajectory instability.

Trajectory instability can be described in terms of the Lyapunov exponents of the system. The largest Lyapunov exponent describes the exponential rate of separation of two phase space trajectories which are generated by the same equations of motion but which originate from two infinitesimally close initial phases (Eckmann and Ruelle 1985). Consider a phase $\boldsymbol{\Gamma}_0$ with another phase $\boldsymbol{\Gamma}_1$, displaced from it at time zero by $\delta\boldsymbol{\Gamma}_1(0)$. If $\delta\boldsymbol{\Gamma}_1(0)$ is infinitessimally small and the system is chaotic, the phase separation evolves as

$$\lim_{t\to\infty} \delta\Gamma_1(t) \approx \exp(\lambda_1 t)\delta\Gamma_1(0)\,, \tag{1}$$

where $\delta\Gamma_1 = |\boldsymbol{\Gamma}_1 - \boldsymbol{\Gamma}_0|$ and $\lambda_1$ is the largest Lyapunov exponent for the system. The largest Lyapunov exponent can be defined as

$$\lambda_1 = \lim_{t\to\infty} \lim_{\delta\Gamma_1\to 0} \frac{1}{2t} \ln\left(\frac{\delta\Gamma_1^2(t)}{\delta\Gamma_1^2(0)}\right). \tag{2}$$

The number of Lyapunov exponents for a system is equal to the dimension of phase space of the system. Therefore an $N$-particle system in three Cartesian dimensions confined to a constant energy hypersurface and with the centre of mass and the total momentum conserved has $6N-7$ Lyapunov exponents. The higher order Lyapunov exponents are defined in terms of the growth of infinitesimally small volume elements of increasing dimension about a phase. Tangent vectors $\delta\boldsymbol{\Gamma}_n$ are defined for each dimension such that they are orthogonal to $\delta\boldsymbol{\Gamma}_m$, where $m = 1, 2, ..., n-1$ and the $n$th volume element is therefore given by $\delta\Gamma_1\,\delta\Gamma_2 \ldots \delta\Gamma_n$. The growth of an infinitessimally small volume element of dimension $n$ is

$$\delta\Gamma_1(t)\,\delta\Gamma_2(t)\ldots\,\delta\Gamma_n(t) \approx \exp[(\lambda_1 + \lambda_2 + \ldots + \lambda_n)t]\delta\Gamma_1(0)\,\delta\Gamma_2(0)\ldots\delta\Gamma_n(0)\,, \tag{3}$$

and the $n$th Lyapunov exponent is given by

$$\lambda_n = \lim_{t\to\infty} \lim_{\delta\Gamma_n\to 0} \frac{1}{2t} \ln\left(\frac{\delta\Gamma_n(t)^2}{\delta\Gamma_n(0)^2}\right). \tag{4}$$

We call the trajectory $\boldsymbol{\Gamma}_0(t)$ the mother trajectory and $\boldsymbol{\Gamma}_1(t), \boldsymbol{\Gamma}_2(t), ..., \boldsymbol{\Gamma}_n(t)$ are called the first, second,..., $n$th daughter trajectories, respectively.

The calculation of the Lyapunov spectrum using equation (4) leads to problems. Taking the $\delta\boldsymbol{\Gamma}_1(0) \to 0$ limit is difficult in numerical work. For finite $\delta\boldsymbol{\Gamma}_1(0)$, if $t \to \infty$ the finite extent of the accessible phase space limits the growth in separation. In order to directly calculate the Lyapunov spectrum using equation (4) it is necessary that the right-hand side of the equation converges before the finiteness of phase space makes itself felt. In order to prevent the exponential growth or shrinking of the tangent vectors periodic rescaling can be carried out (Benettin *et al.* 1976).

Goldhirsch *et al.* (1987) and Hoover and Posch (1985) concurrently developed a differential formulation of the standard method of determining Lyapunov exponents which avoids these problems and has an error of $c_n/t$, where $c_n$ is a constant and $t$ is the length of the finite time simulation (Goldhirsch *et al.* 1987). In this method the phase separation is kept constant using continuous rescaling in a constraint algorithm (Sarman *et al.* 1992). The equations of motion for the displacement vectors of the daughter trajectories, which are constrained to be a fixed distance from the mother trajectory and orthogonal to each other, are given by

$$\delta\dot{\boldsymbol{\Gamma}}_n^{\mathrm{c}} = \boldsymbol{T}\,.\,\delta\boldsymbol{\Gamma}_n^{\mathrm{c}} - \sum_{m<n} \zeta_{nm}\,\delta\boldsymbol{\Gamma}_m^{\mathrm{c}} - \zeta_{nm}\,\delta\boldsymbol{\Gamma}_n^{\mathrm{c}}\,, \tag{5}$$

where

$$\zeta_{nm} = \frac{\delta\boldsymbol{\Gamma}_n^{\mathrm{c}}\,.\,\boldsymbol{T}\,.\,\delta\boldsymbol{\Gamma}_m^{\mathrm{c}} + \delta\boldsymbol{\Gamma}_m^{\mathrm{c}}\,.\,\boldsymbol{T}\,.\,\delta\boldsymbol{\Gamma}_n^{\mathrm{c}}}{(\delta\boldsymbol{\Gamma}_n^{\mathrm{c}})^2}\,, \tag{6}$$

$$\zeta_{nn} = \frac{\delta\boldsymbol{\Gamma}_n^{\mathrm{c}}\,.\,\boldsymbol{T}\,.\,\delta\boldsymbol{\Gamma}_n^{\mathrm{c}}}{(\delta\boldsymbol{\Gamma}_n^{\mathrm{c}})^2}\,. \tag{7}$$

It can be shown (Sarman *et al.* 1992) that the Lyapunov exponents are then related to the constraint force $\zeta_{nn}$ by

$$\lambda_n = \lim_{t\to\infty} \frac{1}{t} \int_0^t \zeta_{nn}\,\mathrm{d}s\,. \tag{8}$$

Molecular dynamics simulations have been used to obtain the full Lyapunov spectra for equilibrium and nonequilibrium systems (Evans *et al.* 1990; Hoover and Posch 1994; Morriss 1989; Sarman *et al.* 1992) with high accuracy. The increase in the computational effort with the number of particles has limited the accurate calculation of the complete Lyapunov spectra to quite small systems at this time. However, in recent work (Hoover and Posch 1994) the full spectrum for 32 and 100 particle systems undergoing colour diffusion or shear flow was calculated.

In order to examine the relationship between Lyapunov instability and the lifetime of antisteady states, we carried out nonequilibrium molecular dynamics simulations of steady states and antisteady states for systems undergoing shear flow. Steady states are produced by thermostatting a system to which an external dissipative field is applied. The complete Lyapunov spectrum of the steady state system with various strain rates was calculated using the constraint algorithm. Antisteady states were produced by applying a time reversal map to steady state phases. We integrated the equations of motion quite accurately and artificially introduce a controlled amount of error at the time the time reversal map is applied.

When a steady state simulation is reversed the entropy production becomes negative. This state is unstable and the system will eventually decay into a stable, entropy producing steady state. Inevitable trajectory error is amplified by Lyapunov instability. If $L(\boldsymbol{\Gamma},\gamma)$ is the Liouville operator (Evans and Morriss 1990) the phase space separation between the forward phase

$$\boldsymbol{\Gamma}_{\mathrm{f}}(t) = \exp[\mathrm{i}\, L(\boldsymbol{\Gamma},\, \boldsymbol{\Gamma})t]\boldsymbol{\Gamma} \qquad (0 < t_{\mathrm{rev}})\,, \tag{9}$$

and the corresponding reversed phase

$$\boldsymbol{\Gamma}_{\mathrm{r}}(t) \equiv \exp[\mathrm{i}\, L(\boldsymbol{\Gamma},\, \gamma)(t_{\mathrm{rev}} - t)]M^{\mathrm{T}}\exp[\mathrm{i}\, L(\boldsymbol{\Gamma},\, \gamma)t_{\mathrm{rev}}]\boldsymbol{\Gamma} \qquad (0 < t < t_{\mathrm{rev}}) \tag{10}$$

obtained by continued time integration of the time reversal mapped phase $M^{\mathrm{T}}\boldsymbol{\Gamma}(t_{\mathrm{rev}})$ is given by $\delta\Gamma(t) \equiv |\boldsymbol{\Gamma}_{\mathrm{r}}(t) - \boldsymbol{\Gamma}_{\mathrm{f}}(t)|$, where $t_{\mathrm{rev}}$ is the time at which the time reversal mapping was applied. From the properties of the time reversal mapping under exact time reversible dynamics, we have $M^{\mathrm{T}}\boldsymbol{\Gamma}_{\mathrm{r}}(t) = \boldsymbol{\Gamma}_{\mathrm{f}}(t)$, $\forall t:\ 0 < t < t_{\mathrm{rev}}$. In this paper we will consider the forward solution of both the mother $\boldsymbol{\Gamma}_0$,

$$\boldsymbol{\Gamma}_{\mathrm{f}0}(t) = \exp[\mathrm{i}\, L(\boldsymbol{\Gamma}_0,\, \gamma)t]\boldsymbol{\Gamma}_0 \qquad (0 < t < t_{\mathrm{rev}})\,, \tag{11}$$

and daughter trajectories $\boldsymbol{\Gamma}_1$,

$$\boldsymbol{\Gamma}_{\mathrm{f}1}(t) = \exp[\mathrm{i}\, L(\boldsymbol{\Gamma}_1,\, \gamma)t]\boldsymbol{\Gamma}_1\,. \tag{12}$$

where $\boldsymbol{\Gamma}_1 = \boldsymbol{\Gamma}_0 + \delta\boldsymbol{\Gamma}_1$. We also follow the reverse time evolution of these trajectories,

$$\boldsymbol{\Gamma}_{\mathrm{r}0}(t) \equiv \exp[\mathrm{i}\, L(\boldsymbol{\Gamma}_0,\, \gamma)(t_{\mathrm{rev}} - t)]M^{\mathrm{T}}\exp[\mathrm{i}\, L(\boldsymbol{\Gamma}_0,\, \gamma)t_{\mathrm{rev}}]\boldsymbol{\Gamma}_0 \qquad (0 < t < t_{\mathrm{rev}})\,, \tag{13}$$

$$\boldsymbol{\Gamma}_{\mathrm{r}1}(t) \equiv \exp[\mathrm{i}\, L(\boldsymbol{\Gamma}_1, \gamma)(t_{\mathrm{rev}} - t)]M^{\mathrm{T}}\exp[\mathrm{i}\, L(\boldsymbol{\Gamma}_1,\, \gamma)t_{\mathrm{rev}}]\boldsymbol{\Gamma}_1 \qquad (0 < t < t_{\mathrm{rev}})\,. \tag{14}$$

Finally we shall consider the following trajectory

$$\boldsymbol{\Gamma}_{\mathrm{r}1'}(t) \equiv \exp[\mathrm{i}\, L(\boldsymbol{\Gamma}_{1'},\, \gamma)(t_{\mathrm{rev}} - t)M^{\mathrm{T}}\boldsymbol{\Gamma}_{1'}\,, \tag{15}$$

with

$$\boldsymbol{\Gamma}_{1'} = \delta\boldsymbol{\Gamma}_{1'} + \exp[\mathrm{i}\, L(\boldsymbol{\Gamma}_0,\, \gamma)t_{\mathrm{rev}}]\boldsymbol{\Gamma}_0 = \delta\boldsymbol{\Gamma}_{1'} + \boldsymbol{\Gamma}_{\mathrm{f}0}(t_{\mathrm{rev}})\,, \tag{16}$$

where a random tangent vector $\delta\boldsymbol{\Gamma}_{1'}$ is added to the mother phase immediately before the time reversal map is applied. This enables us to study the variation of the antisteady state lifetime as a function of integration accuracy.

In a perfectly reversible system, the reverse trajectory exactly retraces the forward trajectory. When noise is present, the displacement of both the forward and the reverse trajectory from their respective perfect trajectories will increase exponentially with rates given by the largest Lyapunov exponent of the forward and the reverse systems respectively. In this work, time reversed simulations were carried out to demonstrate this fact. Furthermore we compare the largest Lyapunov exponent determined from the reverse simulation with the smallest Lyapunov exponent of the forward simulation calculated using the constraint algorithm.

The lifetime of an antisteady state can be characterised by its half-life $t_{1/2}$, which we define as the time required for the ensemble averaged shear stress of the time reversed trajectory to become equal to zero (Evans *et al.* 1991). A relationship between $t_{1/2}$ and the Lyapunov spectrum is developed in this paper by monitoring the divergence of the shear stress from its antisteady state value as a function of strain rate and the noise introduced on time reversal. The divergence in the shear stress of two trajectories whose initial conditions differ by a small amount and are both simulated in the forward direction is also examined.

After time reversal, the Lyapunov spectrum is inverted (i.e. $\lambda_i \to -\lambda_i$) (Eckmann and Ruelle 1985). This means for example that the largest Lyapunov exponent of the antisteady state is $-1$ times the smallest (i.e. most negative) Lyapunov exponent of the steady state. We have exploited this fact to calculate the smallest exponent of steady states which is otherwise a difficult numerical task. This is an efficient method of determining this exponent for systems where the conjugate pairing rule is not valid (Evans *et al.* 1991).

## 2. Simulations

Nonequilibrium molecular dynamics (NEMD) simulations of shear flow were carried out to study the influence on Lyapunov stability on the lifetime of antisteady states. The simulations were carried out in two Cartesian dimensions with a constant temperature maintained using a Gaussian thermostat (Evans and Morriss 1990). (Reduced units are used throughout this paper.)

The equations of motion employed were the SLLOD equations (Evans and Morriss 1990) which are given by

$$\dot{\boldsymbol{q}}_i = \boldsymbol{p}_i + \boldsymbol{i}\gamma y_i, \qquad \dot{\boldsymbol{p}}_i = \boldsymbol{F}_i - \boldsymbol{i}\gamma p_{yi} - \alpha\boldsymbol{p}_i\,, \tag{17}$$

where $\gamma$ is the strain rate and $\alpha$ is the thermostat multiplier

$$\alpha = \sum_{i=1}^{N} \boldsymbol{F}_i \cdot \boldsymbol{p}_i - \gamma p_{xi} p_{yi} \Big/ \sum_{i=1}^{N} \boldsymbol{p}_i^2 . \tag{18}$$

The shear stress of the system is $-P_{xy}$, where $P_{xy}$ is the $xy$ element of the pressure tensor which is given by

$$P_{xy} V = \sum_{i=1}^{N} p_{xi} p_{yi}/m - \tfrac{1}{2} \sum_{ij}^{N} x_{ij} F_{yij} . \tag{19}$$

A Lees–Edwards periodic system of eight WCA disks (Evans and Morriss 1990) was examined at a temperature of $T = 1\cdot 0$ and a particle density of $n = 0\cdot 4$.

**Table 1. Strain rate dependence of the Lyapunov exponents and the rate of increase in the difference in shear stress of trajectories**

| $\gamma$ | $\lambda_{\max}$ | $\lambda_{\min}$ | Rate of increase in shear stress difference A | B | C | D |
|---|---|---|---|---|---|---|
| 0·1 | 2·19(5) | −2·19(6) | 2·12(4) | 2·15(2) | 2·16(3) | 2·149(9) |
| 1·0 | 2·13(2) | −2·59(6) | 2·14(2) | 2·55(2) | 2·58(3) | 2·56(2) |
| 2·0 | 2·15(5) | −3·64(13) | 2·09(3) | 3·584(9) | 3·62(8) | 3·60(4) |
| 3·0 | 2·23(6) | −5·75(11) | 2·13(8) | 5·49(2) | 5·48(35) | 5·37(26) |

$\mathrm{A} = \mathrm{d}\langle \ln|P_{xy}(\boldsymbol{\Gamma}_{\mathrm{f}l}) - P_{xy}(\boldsymbol{\Gamma}_{\mathrm{f}0})|\rangle/\mathrm{d}t$, $\mathrm{B} = \mathrm{d}\langle \ln|(\boldsymbol{\Gamma}_{rl'}(t) - \boldsymbol{\Gamma}_{\mathrm{f}0}(t))|\rangle/\mathrm{d}t$,

$\mathrm{C} = \mathrm{d}\langle \ln|P_{xy}(\boldsymbol{\Gamma}_{rl'}) - P_{xy}(\boldsymbol{\Gamma}_{\mathrm{f}0})|\rangle/\mathrm{d}t$, $\mathrm{D} = \mathrm{d}\langle \ln|P_{xy}(\boldsymbol{\Gamma}_{\mathrm{r}0}) - P_{xy}(\boldsymbol{\Gamma}_{\mathrm{f}0})|\rangle/\mathrm{d}t$.

## 3. Results

Full Lyapunov spectra for steady state systems with various strain rates were determined using the constraint algorithm (Sarman *et al.* 1992). The largest and smallest exponents are shown in the second and third columns respectively of Table 1. Whereas the largest Lyapunov exponent is weakly dependent on the strain rate, the smallest Lyapunov exponent is observed to vary significantly with strain rate.

The time evolution of the absolute value of the difference in the shear stress for pairs of steady state trajectories which are initially close was examined. A nonequilibrium molecular dynamics simulation was used to produce a steady state at the required strain rate. At some time, a displaced phase was formed by adding random noise $\delta\boldsymbol{\Gamma}_{1'}$ in the range $-1\times10^{-4}$ to $1\times10^{-4}$ to each component of the phase. Both trajectories were then simulated (forward in time) and the difference in their shear stress was monitored. It was found that the ensemble average of the absolute value of the difference in the shear stress grows exponentially with a rate given by the largest Lyapunov exponent of the steady state, $\lambda_{\max}^{\mathrm{ss}}$. This is demonstrated in Fig. 1 which shows the time evolution of the shear stress separation obtained from nonequilibrium molecular dynamics simulations of a steady state system with of strain rates of $0\cdot 1$ and $3\cdot 0$. After initial alignment

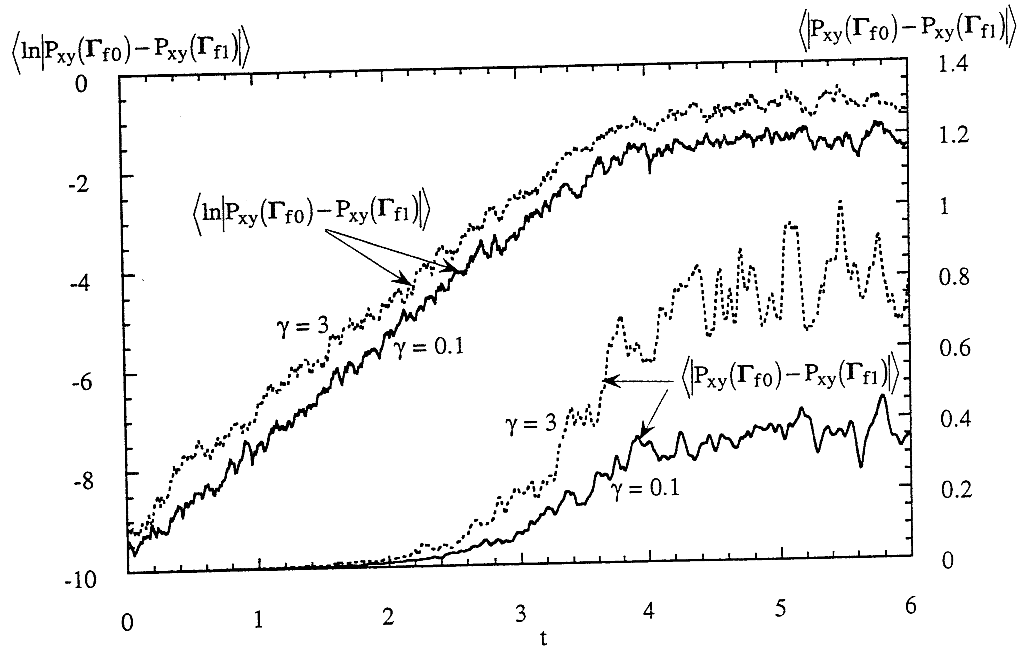


**Fig. 1.** Time evolution of the ensemble average absolute value of the difference in the shear stress of two trajectories which are initially close. The system is undergoing steady shear flow at $T = 1 \cdot 0$ and $n = 0 \cdot 4$. The results obtained with a strain rate of $\gamma = 0 \cdot 1$ are given by the solid curves, whereas those for $\gamma = 3 \cdot 0$ by the dotted curves.

of the displacement vectors, the separation increases exponentially with growth rates of $2 \cdot 12(4)$ for $\gamma = 0 \cdot 1$ and $2 \cdot 13(8)$ for $\gamma = 3 \cdot 0$, which are equal to the largest Lyapunov exponent for the steady state at the specified strain rate (see column A in Table 1). After approximately $t = 3 \cdot 0$, the growth becomes inhibited due to the finite momentum space $(\sum p_i^2/2m = NkT)$.

An unstable antisteady state is produced when time reversal is carried out on a typical steady state phase. The antisteady state is maintained until noise results in departure of the trajectory from the antisteady state to a steady state. In order to demonstrate this, nonequilibrium steady states with various strain rates were produced and steady state trajectories recorded from $t = 0$ to $t = 10$. Each trajectory was then simulated in the reverse direction with noise $\delta \boldsymbol{\Gamma}_{1'}$ introduced on time reversal (i.e. $t_{\text{rev}} = 10$) and the phase separation of the forward and reverse trajectories was calculated. Fig. 2 shows the time evolution of the separation of simulated reverse trajectories from their forward trajectories and the influence of the magnitude of the noise introduced on time reversal for a system with $\gamma = 1 \cdot 0$. The growth in the separation is exponential until the effect of the finite nature of momentum space is felt.

The fifth column of Table 1 gives the rate of exponential growth of the phase space separation at various strain rates. Comparison with the Lyapunov exponents at these strain rates (shown in the second and third columns of Table 1) confirms that the rate of this exponential separation is equal to the negative of

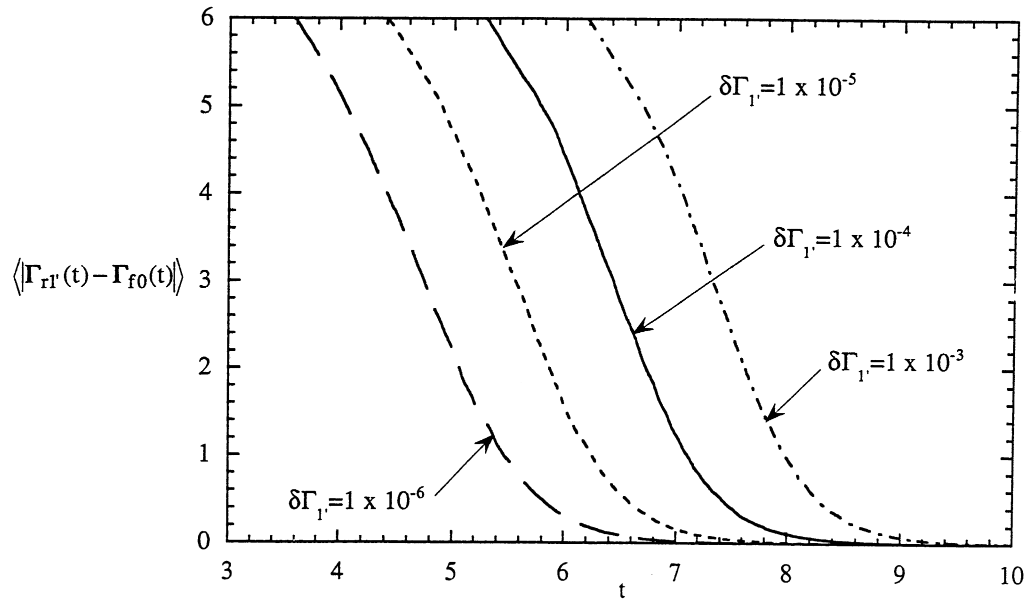


**Fig. 2.** Time evolution of the deviation of a time reversed trajectory from the forward trajectories due to noise introduced at time reversal ($t_{rcv} = 10\cdot0$). The system is undergoing shear flow at $T = 1\cdot0$, $n = 0\cdot4$ and $g = 1\cdot0$. Each curve is labelled with the magnitude of the maximum noise introduced at time reversal.

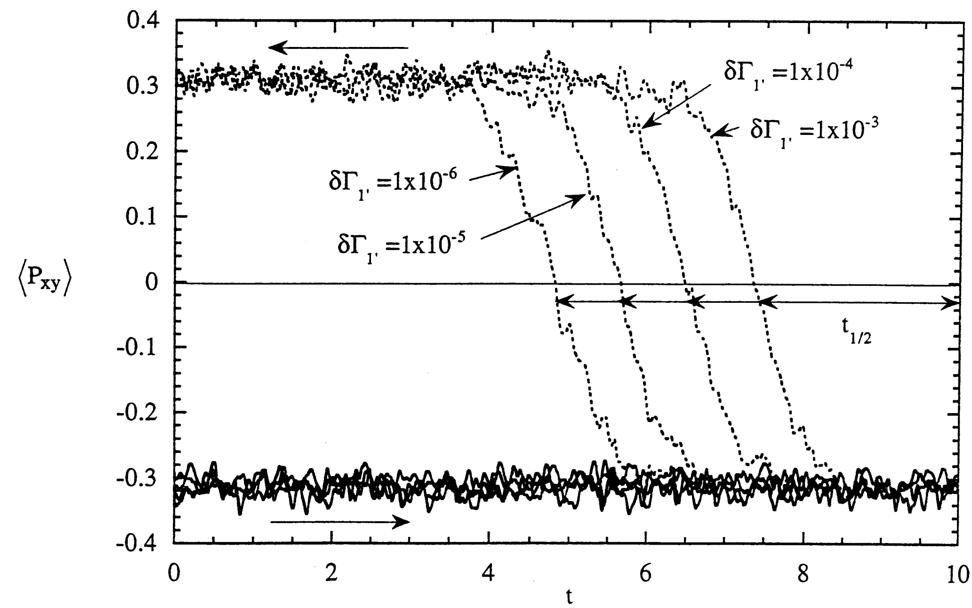


**Fig. 3.** Time evolution of the shear stress for steady states which are reversed at $t_{rcv} = 10\cdot0$ and the influence of noise introduced at time reversal. The system is undergoing shear flow with $T = 1\cdot0$, $n = 0\cdot4$ and $g = 1\cdot0$. The results for the forward simulations are given by solid curves and the reverse simulations are given by the dotted curves. Each set of data from the time-reversed simulation is labelled with the magnitude of the maximum noise introduced at time reversal.

the smallest Lyapunov exponent for the steady state or, equivalently, the largest exponent of the antisteady state, $-\lambda^{ss}_{min}$ $(= \lambda^{ass}_{max})$.

Fig. 3 shows the response of the ensemble averaged shear stress after time reversal with $\gamma = 1{\cdot}0$. Random noise $\delta\boldsymbol{\Gamma}_{1'}$ was introduced to all phase space coordinates on time reversal and the influence of the magnitude of this noise is shown. Initially the separation is exponential and the rate of exponential growth for the system is given in Table 1. From Table 1 it is clear that the rate of increase is equal to the smallest Lyapunov exponent for the steady state, $-\lambda^{ss}_{min}$ $(= \lambda^{ass}_{max})$. The rate of increase obtained when no noise is introduced (D) on time reversal (that is $\boldsymbol{\Gamma}_{\mathrm{r}1'} \to \boldsymbol{\Gamma}_{\mathrm{r}0}$) is also shown in Table 1 and is equal to the smallest Lyapunov exponent for the steady state. In this case all errors are due to the finite accuracy of the computer simulation.

A simulated forward trajectory separates from an exact forward trajectory at a rate given by the largest Lyapunov exponent of the steady state and the simulated reverse trajectory separates from an exact reverse trajectory at a rate given by the smallest Lyapunov exponent for the steady state. Therefore it might be anticipated that the separation of the reverse simulated trajectory from the forward simulated trajectory would be influenced by both the largest and smallest Lyapunov exponent of the steady state. In the computer simulations only an

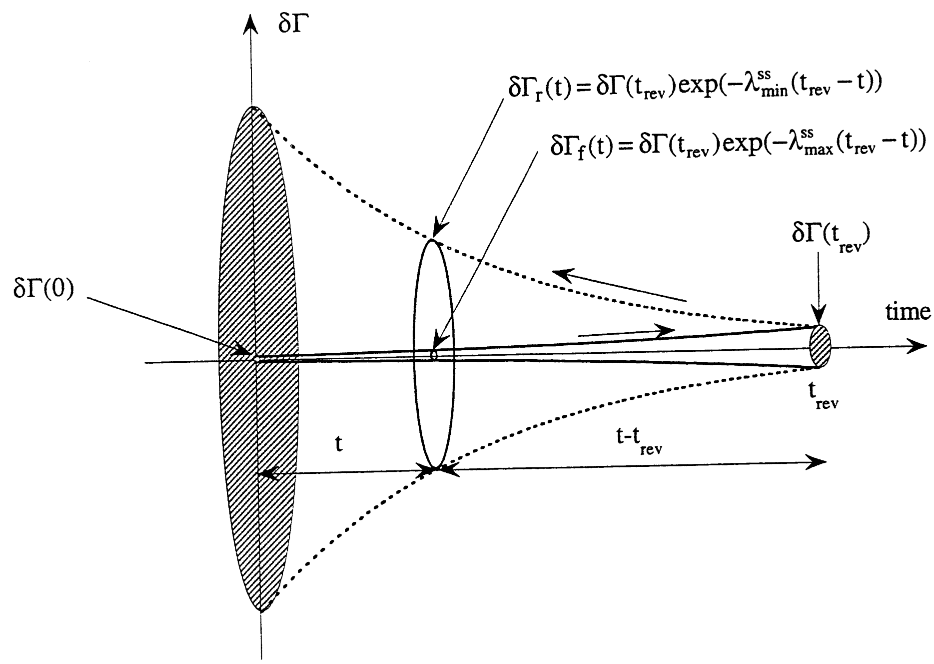


**Fig. 4.** A schematic diagram depicting the change in distance of the simulated trajectory from the exact trajectory which starts at $t = 0$. For the forward simulation the magnitude of the tangent vector $\delta\Gamma_{\mathrm{f}}(t)$, increases exponentially with a rate given by the largest Lyapunov exponent of the steady state $\lambda^{ss}_{max}$, whereas the magnitude of the tangent vector for the reverse simulation $\delta\Gamma_{\mathrm{r}}(t)$ increases at a rate given by the smallest Lyapunov exponent of the steady state $-\lambda^{ass}_{min}$. Clearly, separation of the reverse simulated and forward simulated trajectories will be dominated by the influence of the separation of the reverse trajectory from the exact trajectory when $0 < t < t_{\mathrm{rev}}$.

influence due to the smallest Lyapunov exponent is observed. The reason for this observation is demonstrated in Fig. 4 and is due to the dominant influence of the smallest Lyapunov exponent when $t < t_{\rm rev}$.

In Fig. 4 we give a schematic diagram of the time evolution of the error 'cones' $\delta\Gamma$ for the forward and reverse trajectories. The ensemble averaged phase separation of the forward and from the corresponding reversed trajectory as a function of time can be estimated as the mean separation of phase points inside the trajectory cones at a specific time. As the time after reversal increases the error cone of the antisteady state increases in radius while the corresponding error cone for the steady state actually *decreases*. So at long times the separation of the forward and reversed trajectories is

$$\delta\Gamma \sim \delta\Gamma(t_{\rm rev})\{\exp[-\lambda_{\rm max}^{\rm ass}(t-t_{\rm rev})] + \exp[-\lambda_{\rm min}^{\rm ss}(t-t_{\rm rev})]\}$$

$$\sim \delta\Gamma(t_{\rm rev})\exp[-\lambda_{\rm min}^{\rm ss}(t-t_{\rm rev})],$$

which is dominated by the largest Lyapunov exponent of the antisteady state.

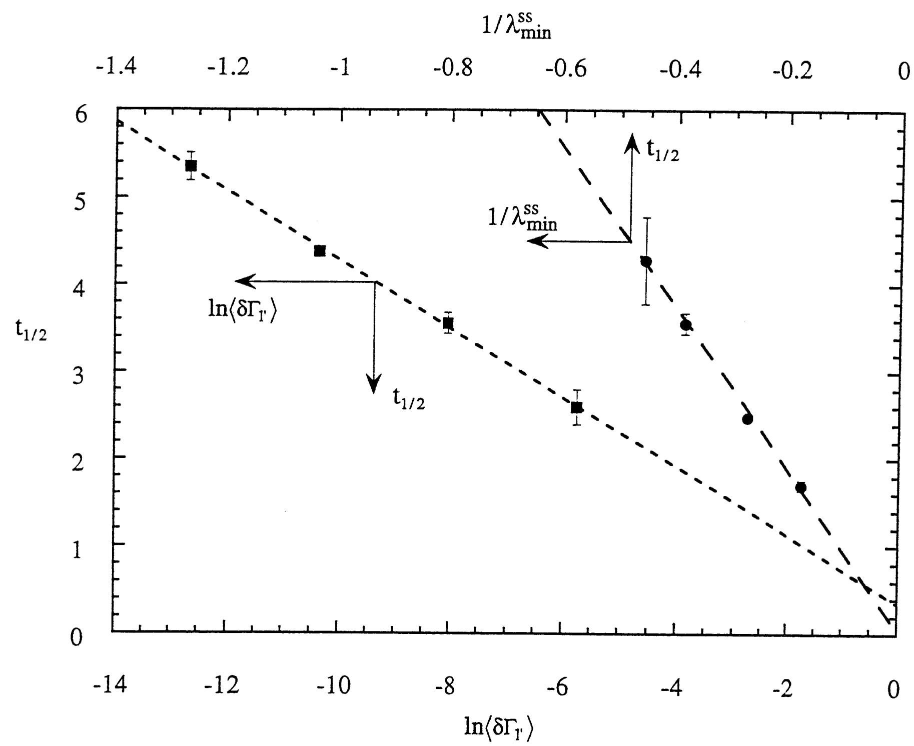


**Fig. 5.** Dependence of the half-life of the antisteady state on both the initial noise, $\delta\Gamma_{1'}$ at a constant strain rate of $\gamma = 1\cdot0$ (squares) and on the smallest Lyapunov exponent $\lambda_{\rm min}^{\rm ass}$ of the steady state system with a constant initial trajectory error of $\ln\langle\delta\Gamma_{\rm r}\rangle = -8\cdot05$ (circles). The lines are least squares fits to the data. The system is undergoing shear flow at $T = 1\cdot0$ and $n = 0\cdot4$.

The half-life of the anti-steady state is given by the time required for the shear stress to become zero (see Fig. 3). The half-life decreases as the noise $\delta\boldsymbol{\Gamma}_{1'}$ is increased and as $\lambda^{\rm ss}_{\rm min}$ of the steady state decreases. We increase the magnitude of the minimum steady state Lyapunov exponent by simply increasing the strain rate. Fig. 5 shows that $t_{1/2}$ decreases linearly with the logarithm of the noise introduced and is inversely proportional to $\lambda_{\rm min}$ giving a relationship of $t_{1/2} = -\{\ln(k) - \ln(\delta\Gamma(t_{\rm rev}))\}/\lambda^{\rm ss}_{\rm min}$. This relationship is easily derived when we recognise that the steady state is likely to decay when the Lyapunov amplified noise $\delta\Gamma(t)$ becomes a significant fraction of the average interparticle separation and momentum, so that $\delta\Gamma(t_{1/2}) = k$. We therefore have $k = \delta\Gamma(t_{\rm rev})\exp(-\lambda^{\rm ss}_{\rm min}\, t_{1/2})$ and simulations show $k = 3{\cdot}0{\pm}0{\cdot}2$.

## 4. Conclusions

Using nonequilibrium molecular dynamics simulations of an eight particle two-dimensional system undergoing shear flow we have demonstrated the effects of Lyapunov instability on the separation of phase space trajectories and on the reversibility of the system. The rate of exponential growth of the separation of trajectories is given by the largest Lyapunov exponent of the ergodic system, while the rate of separation of a reversed trajectory from its forward path is given by the negative of the smallest Lyapunov exponent for the system simulated in the forward direction.

Antisteady states can be created by taking a phase point from a steady state and simulating backwards in time. This state violates the Second Law of Thermodynamics and, due to Lyapunov instability, will eventually form a Second Law satisfying steady state if noise is introduced. The half-life of an antisteady state can be related to the noise introduced to the system and is increased by reducing noise. The half-life is infinite when no noise is introduced.

The dependence of the half-life of the antisteady state on the smallest Lyapunov exponent of the steady state has been demonstrated. It was found that the half-life is inversely proportional to the smallest Lyapunov exponent of the steady state. Since the smallest Lyapunov exponent is negative and decreases with strain rate, this results in a decrease in the half-life with an increase in strain rate for shearing systems.

## References

Benettin, G., Galgani, L., and Strelcyn, J.-M. (1976). *Phys. Rev.* A **14**, 2338–45.

Eckmann, J.-P., and Ruelle, D. (1985). *Rev. Mod. Phys.* **57**, 617–56.

Evans, D. J., Cohen, E. G. D., and Morriss, G. P. (1990). *Phys. Rev.* A **42**, 5990–7.

Evans, D. J., and Morriss, G. P. (1990). 'Statistical Mechanics of Nonequilibrium Liquids' (Academic: New York).

Evans, D. J., Sarman, S., Baranyai, A., Cohen, E. G. D., and Morriss, G. P. (1991). Proc. Conf. on Microscopic Simulations of Complex Hydrodynamical Phenomena, Alghero, NATO ASI Series B, Vol. 292, pp. 285–99 (Plenum: New York).

Goldhirsch, I., Sulem, P.-L., and Orszag, S. A. (1987). *Physica* D **27**, 311–37.

Hoover, W. G., and Posch, H. A. (1985). *Phys. Lett.* A **113**, 82–4.

Hoover, W. G., and Posch, H. A. (1994). *Phys. Rev.* E **49**, 1913–20.

Morriss, G. P. (1989). *Phys. Lett.* A **134**, 307–13.

Sarman, S., Evans, D. J., and Morriss, G. P. (1992). *Phys. Rev.* A **45**, 2233–42.

Manuscript received 10 May, accepted 21 June 1995